Measurements of debris flow entrainment and dynamics

Hervé Vicari[1,2*], *Charles W. W.* Ng[3], *Steinar* Nordal[4], *Vikas* Thakur[4], *W. A. Roanga K.* De Silva[3], *Haiming* Liu[3], and *Clarence E.* Choi[5]

[1]Norwegian Geotechnical Institute (NGI), Natural Hazards section, Oslo, Norway
[2]Current affiliation: WSL Institute for Snow and Avalanche Research SLF, Davos, Switzerland
[3]Hong Kong University of Science and Technology (HKUST), Hong Kong
[4]Norwegian University of Science and Technology (NTNU), Civil and Environmental Engineering, Trondheim, Norway
[5]Hong Kong University (HKU), Hong Kong

Abstract. The mechanisms of debris flows and their interaction with mitigation structures are still not well understood. Among the research challenges, only few entrainment measurements are available in literature, as entrainment is often masked by deposition on top. In this paper, we present a simple, cheap, and effective method to measure the entrainment depths. Flume experiments have therefore been performed to assess the influence of the initial debris flow volume and of an upstream flexible barrier on entrainment. To better understand the debris flow dynamics, the flow basal stresses have been measured. A high degree of liquefaction at the base of the debris flow is observed. A mitigation measure to reduce entrainment has also been studied. A compact flexible barrier was installed in the upstream part of the channel and is observed to deflect the flow along a curvilinear path. High normal stresses are measured at the base of the overflow, which are caused by the additional centrifugal stresses from the overflow. The results from the flume tests suggest that the flow interaction with an upstream flexible barrier may significantly influence the debris flow dynamics both upstream and downstream of the barrier.

1 Introduction

Debris flows typically increase in scale by entraining soil, fluid and boulders along the flow path. The entrainment process may significantly influence the debris flow dynamics, due to the increase of the debris flow volume [1] and to the generation of excess pore pressures in the erodible bed [2]. To understand and model debris flow entrainment, reliable measurements of the entrainment depths are needed. Some methods have been proposed in literature to measure debris flow entrainment. For instance, laser technologies have been applied [3] to measure the net erosion (difference between erosion and deposition depth). In this case, however, entrainment cannot be distinguished from deposition. Electronic sensors have been successfully applied to measure the entrainment depths [4,5]. However, they may be complex and expensive to install in the field. In this work, we describe a simple but effective methodology to measure the entrainment depths, which is applied in large-scale flume experiments.

The development of excess pore pressures within the debris flow may also significantly affect the flow basal stresses and therefore the dynamics of debris flows [6]. Hence, flow basal stresses are measured in the large-scale flume tests and compared to values in literature. Furthermore, the presence of mitigation measures such as flexible barriers may also significantly affect the debris flow dynamics. In this work we report measurements of the flow basal stresses affected by a compact flexible barrier.

2 Methodology

2.1 Physical flume modelling

Large-scale flume experiments were conducted by Vicari et al. (2021) to study the entrainment of a wet soil bed by a debris flow [7]. Fig. 1 shows the 28 m-long flume [8] which was used to perform the tests. Initial volumes of wet debris of 2.5 and 6 m^3 were placed in a storage container. The debris could be triggered by dam-break, by opening a 1 m-tall door. The debris material was then flowing along a 15 m-long 2 m-wide channel inclined at 20°. The base of the initial part of the channel (9 m) is fixed (non-erodible), which allowed the flow to develop and acquire a typical elongated shape. Wet soil was placed over the last 6 m of the inclined channel and has a thickness of 120 mm. The inclined channel ends in a horizontal 4.4 m-long runout section. At the end of the runout section, a terminal flexible barrier was placed to arrest the flowing mass. Instrumentation was placed in the channel to measure flow depths and velocities, basal stresses, and entrainment depths along the erodible bed. Three tests were performed (Table 1), The first two tests were executed without any upstream barrier, with initial volumes of 2.5 and 6 m^3 respectively. In the third test, a 0.6 m-tall flexible barrier was placed at 4.3 m from the

* Corresponding author: herve.vicari@slf.ch

gate, to study the effect of an upstream flexible barrier on entrainment reduction.

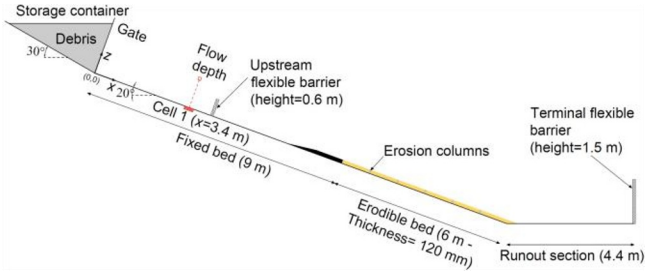

Fig. 1. Flume model.

Table 1. Test program.

Test ID	Release flow volume (m^3)	Flexible barriers setup
V2.5-B1	2.5	Terminal flexible
V6-B1	6	Terminal flexible barrier
V6-B2	6	Upstream + Terminal flexible barriers

2.2 Instrumentation to measure the entrainment depth

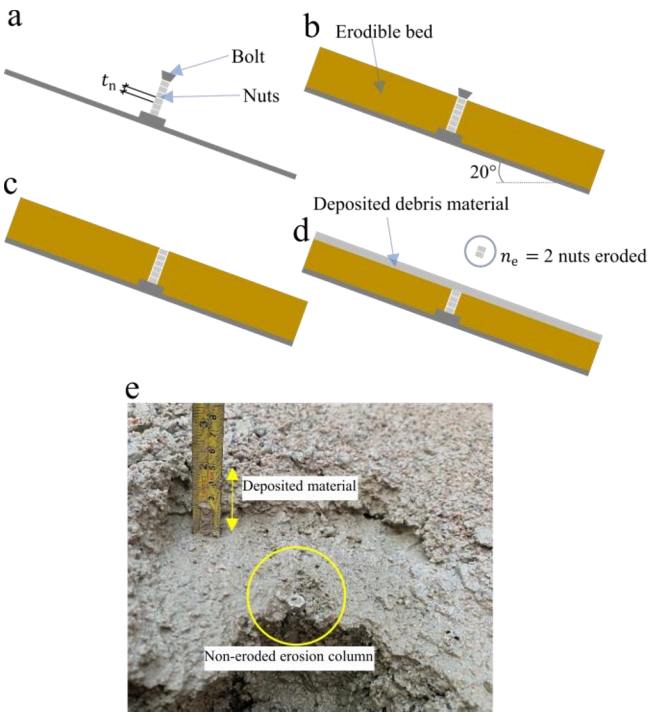

Fig. 2. Erosion column designed by [7].

A technique has been developed in [7] to measure the entrainment depths along the erodible bed (Fig. 2) allowing to differentiate entrainment from deposition. Columns of nuts are installed through a bolt into the erodible bed prior to its construction (Fig. 2a). The soil bed is then prepared (Fig. 2b). Afterwards, the bolts are removed, and the nuts are therefore free to be entrained with the erodible bed (Fig. 2c). After the test, the number of nuts entrained, n_e, at each column location is counted (difference between initial number of nuts and nuts left in place) (Fig. 2d), which allows the calculation of the entrainment depth, e:

$$e = n_e \cdot t_n \quad (1)$$

where t_n is the thickness of each nut (in the experiments, 5 mm). The deposition depth is also measured after each test, as the debris thickness above the remaining nuts. Fig. 2e shows an erosion column after a test. A similar instrumentation to measure entrainment was also successfully used in small-scale experiments by [9,10].

3 Test results and discussion

3.1 Entrainment depths

Fig. 3 shows the measured entrainment depths for the three tests. The entrainment is typically higher at the start of the erodible bed, due to a ploughing entrainment mechanism [11,12]. Entrainment depths for test V6-B1 are higher compared to the entrainment depths of test V2.5-B1, which is due to a higher initial volume (6 m^3 vs. 2.5 m^3 respectively).

Conversely, in test V6-B2, the lowest entrainment depths are measured. Indeed, the upstream flexible barrier retained part of the initial volume (1.2 m^3), dissipated energy and reduced the flow velocity. Furthermore, the upstream flexible barrier was observed to split the flow into two distinct surges, which eroded significantly less bed material compared to the other two tests.

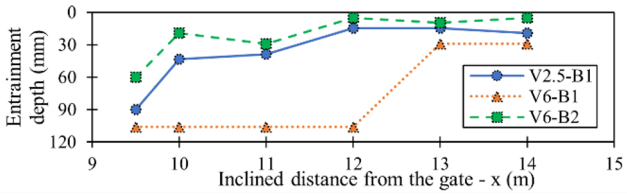

Fig. 3. Measured entrainment depths in [7].

3.2 Flow basal stresses

A load cell was installed at the base of the flume bed at 3.4 m from the gate to measure both the normal and shear stresses. The load cell was connected to a surface plate which is roughened through epoxy and sand. On top of the load cell, an ultrasonic sensor measures the flow depth normal to the slope.

Fig. 4a and 4b show the measured flow depth and basal stresses for tests V6-B1 and V6-B2 respectively. In test V6-B1, the measured normal stress is observed to have a similar trend and shape compared to the measured flow depth. The normal stress can be modelled by considering the static equilibrium of a debris flow column perpendicular to the channel bed:

$$\sigma_{n,stat} = \rho_f \, g \, h_f \cos\theta \quad (2)$$

where ρ_f is the debris flow density (measured equal to 2155 kg/m3, based on the flow composition), g is the acceleration due to gravity, h_f is the flow depth and θ is

the slope angle (20°). Therefore, the calculated normal stress is approximately equal to:

$$\sigma_{n,stat} \cong 20\ h_f \quad (3)$$

with h_f measured in [m] and $\sigma_{n,stat}$ in [kPa]. Hence, reading the flow depth on the left y-axis provides the calculated theoretical normal stress according to Eq. 3. It can be observed that for test V6-B1, the theoretical prediction of the normal stress is quite in agreement with the measured normal stress.

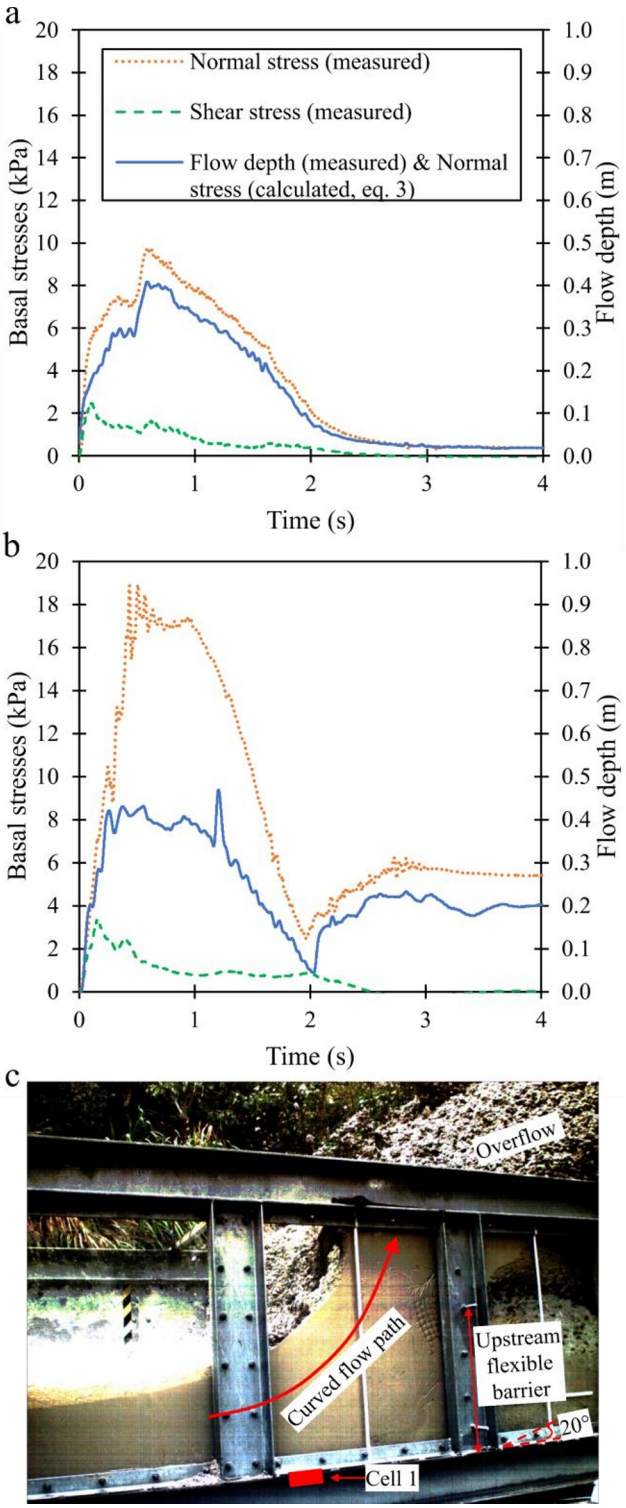

Fig. 4. Measured flow basal stresses and flow depth in [7] for (a) test V6-B1; (b) test V6-B2. (c) Run-up impact mechanism on the upstream flexible barrier for test V6-B2.

Instead, in test V6-B2, the flow measured normal stress is significantly higher compared to the measured flow depth. To explain the measurement, the kinematics of the flow impacting the upstream flexible barrier is shown in Fig. 4c. It is observed that a curvilinear overflow develops, which induces centrifugal stresses normal to the topography and therefore to the load cell. The centrifugal stress may be calculated as proposed by [13]:

$$\sigma_{n,centrifugal} = k\ \rho_f\ h_f\ v_f^2 \quad (4)$$

where k is the curvature of the flow path and v_f is the velocity of the overflowing layer. Based on video analysis of the experiments, the following values of the flow parameters are assumed: $k \cong 1.1\ m^{-1}$, $h_f \cong 0.2$ m, $v_f \cong 5$ m/s. Using these values, $\sigma_{n,centrifugal} \cong 12$ kPa is calculated. Adding the centrifugal component to the calculated static basal stress ($\sigma_{n,stat} \cong 8$ kPa) results in a total normal stress of approximately 20 kPa which is similar to the measured normal stress in test V6-B2. This result shows that a compact upstream flexible barrier may significantly alter the flow dynamics.

The measured shear stress in Fig. 4a and 4b does not follow the same trend as the measured flow depth and normal stress. A frictional behaviour is assumed to model the flow basal shear stress through the Mohr-Coulomb model:

$$\tau_{f\text{-}b} = \sigma_n \tan(\varphi_{f\text{-}b}) \quad (5)$$

where $\varphi_{f\text{-}b}$ is an apparent friction angle at the base of the flow, which implicitly accounts for the effect of pore pressures on shear strength reduction (notice indeed that the total normal stress σ_n is used in Eq. 5). $\varphi_{f\text{-}b}$ is therefore calculated from Eq. 5, based on the measured shear and normal stresses, and shown in Fig. 5. At the flow front, high values of $\varphi_{f\text{-}b}$ are calculated (15° to 40°), which suggests faster dissipation of excess pore pressures. Instead, the body of the flow is characterized by a lower apparent friction angle $\varphi_{f\text{-}b}$ (5° to 15°), which suggests significant liquefaction. This observation agrees with the experimental results by [14].

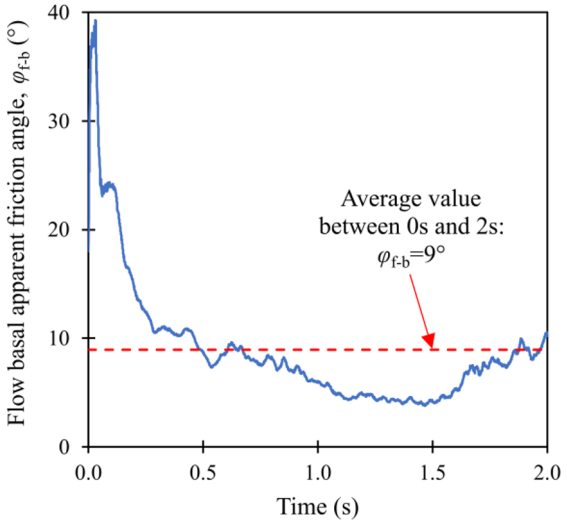

Fig. 5. Calculated flow basal apparent friction for test V6-B1 [11].

The average apparent friction angle is calculated as $\bar{\varphi}_{f\text{-}b} \cong 9°$. Table 2 compares the flow basal apparent friction angle $\varphi_{f\text{-}b}$ calculated from different studies (flume tests and in situ data). In general, the measured $\varphi_{f\text{-}b}$ is quite lower compared to the effective friction angle of poorly sorted soil material which is typical of debris flow ($\varphi' \cong 30° - 40°$). This observation suggests the significance of liquefaction during the debris flow dynamics. In table 2, back-calculated values of $\varphi_{f\text{-}b}$ for real debris flow events using a depth-averaged model are also reported. The range of back-calculated apparent friction is similar to the measured values of $\varphi_{f\text{-}b}$, which suggests that flume experiments are relevant to study the mechanical processes of real debris flow events.

Table 2. Literature values of debris flow basal apparent friction.

Study	Debris flow basal apparent friction, $\varphi_{f\text{-}b}$ (°)
[15] – Illgraben debris flow channel	~ 6
[14] – sand+gravel mixture on rough bed	~ 19
[14] – sand+gravel+mud mixture on rough bed	~ 0
[14] – sand+gravel mixture on smooth bed	~ 0
[7] – This study	~ 9
[16] - Back-calculation of several full-scale debris flows using a depth-averaged model	3 - 13

4 Conclusions

The following conclusions can be drawn:
- A simple but effective instrumentation, "erosion columns", has been designed and tested. This technique offers the possibility to instrument real debris flow channels, which may improve our understanding on the entrainment mechanisms.
- The presence of a compact flexible barrier increases the flow basal stresses upstream of the barrier owing to the formation of a curvilinear flow.
- The measured flow basal stresses are used to calculate the flow basal apparent friction angle, which suggests a significant liquefaction in the flow body.

The authors are grateful to Centre for Research Driven Innovation (CRI) KLIMA2050 and INTPART project "Landslide Mitigation of Urbanized Slopes for Sustainable Growth", funded by the Research Council of Norway. The authors are also grateful for the financial sponsorship from the Research Grants Council of Hong Kong SAR, China (AoE/E-603/18). W.A.R.K. De Silva gratefully acknowledges the support of Hong Kong PhD Fellowship scheme (HKPFS) provided by the RGC of HKSAR.

References

1. A. Mangeney, O. Roche, O. Hungr, N. Mangold, G. Faccanoni, A. Lucas, J. Geophys. Res. Earth Surf. **115**, 1 (2010).
2. R. M. Iverson, J. Geophys. Res. Earth Surf. **117**, 1 (2012).
3. P. Schürch, A. L. Densmore, N. J. Rosser, B. W. McArdell, Geology **39**, 827 (2011).
4. R. M. Iverson, M. E. Reid, M. Logan, R. G. LaHusen, J. W. Godt, J. P. Griswold, Nat. Geosci. 4, **116** (2011).
5. C. Berger, B. W. McArdell, F. Schlunegger, J. Geophys. Res. Earth Surf. **116**, 1 (2011).
6. R. M. Iverson, Rev. Geophys. **35**, 245 (1997).
7. H. Vicari, C. W. W. Ng, S. Nordal, V. Thakur, W. A. R. K. De Silva, H. Liu, C. E. Choi, Can. Geotech. J. **59**, 6 (2021).
8. C. W. W. Ng, C. E. Choi, U. Majeed, S. Poudyal, W. A. R. K. de Silva, *Fundamental Framework to Design Multiple Rigid Barriers for Resisting Debris Flows*, 16th Asian Reg. Conf. Soil Mech. Geotech. Eng. ARC 2019 1 (2019).
9. J. Du, C. E. Choi, J. Yu, V. Thakur, J. Geophys. Res. Earth Surf. **127**, 1 (2022).
10. P. Song, C. E. Choi, J. Geophys. Res. Earth Surf. **126**, 1 (2021).
11. H. Vicari, Q. A. Tran, S. Nordal, V. K. S. Thakur, Landslides **19** (2022).
12. H. Vicari, Q. A. Tran, S. Nordal, V. K. S. Thakur, *MPM Simulations of Debris Flow Entrainment, Modelling Boulders Explicitly*, in Geohazards 8, 12-15 June 2022, Québec, Canada (2022).
13. O. Hungr, Can. Geotech. J. **32**, 610/623 (1995).
14. R. M. Iverson, M. Logan, R. G. LaHusen, M. Berti, J. Geophys. Res. **115**, F03005 (2010).
15. B. W. McArdell, P. Bartelt, J. Kowalski, Geophys. Res. Lett. **34**, 2 (2007).
16. K. Schraml, B. Thomschitz, B. W. Mcardell, C. Graf, R. Kaitna, Nat. Hazards Earth Syst. Sci. **15**, 1483 (2015).